THIS MONTH IN
JNM

Non–probe-based imaging of apoptosis: Blankenberg and Strauss continue their focus on cell death imaging, this time looking at existing nonradionuclide clinical modalities, including ultrasound, MR, and optical imaging. . . . . ***Page 1***

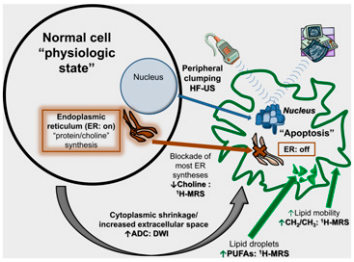

PET/CT in LABC: Groheux and colleagues study the effectiveness and impact of ^{18}F-FDG PET/CT on initial staging in locally advanced breast cancer, including patients with both noninflammatory and inflammatory disease. . . . . ***Page 5***

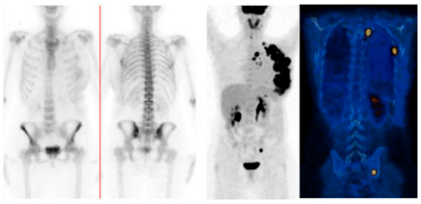

Dynamic PET/CT in pancreatic cancer: Epelbaum and colleagues assess the role of a quantitative dynamic ^{18}F-FDG PET/CT model in pancreatic cancer as a potential index of tumor aggressiveness and predictor of survival. . . . . ***Page 12***

PET textural features as predictors: Cook and colleagues explore the question of whether textural features of non–small cell lung cancer tumoral uptake in ^{18}F-FDG PET images are correlated with patient survival and response to chemoradiotherapy. . . . . ***Page 19***

MTV and anal cancer outcomes: Bazan and colleagues evaluate the prognostic potential of metabolic tumor volumes derived from PET in patients treated with definitive chemoradiotherapy for anal cancer. . . . . ***Page 27***

^{177}Lu-DOTA-octreotate dosimetry: Sandström and colleagues describe the development of an individualized dosimetry protocol for bone marrow in ^{177}Lu-octreotate therapy and a process for individualized absorbed kidney/bone marrow dose calculation to optimize therapy. . . . . ***Page 33***

^{18}F-FDOPA PET in neuroblastic tumors: Lu and colleagues assess the accuracy and potential role of ^{18}F-FDOPA PET in patients with neuroblastic tumors and compare results with those from ^{18}F-FDG PET and ^{123}I-MIBG scintigraphy. . . . . ***Page 42***

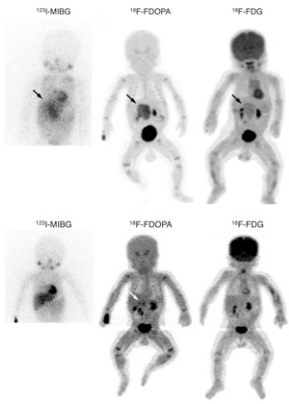

Misregistration and flow estimation: Rajaram and colleagues study the effects of misregistration of cardiac PET/CT data on quantification of myocardial blood flow in patients with normal blood flow. . . . . ***Page 50***

Quantitative PET/CTCA accuracy: Danad and colleagues investigate the diagnostic accuracy of quantitative $H_2{}^{15}O$ PET/CT-based coronary angiography in patients with suspected coronary artery disease and compare results with those from PET- or CT-based data alone. . . ***Page 55***

Propofol and ^{11}C-PBR28 binding: Hines and colleagues analyze the effect in healthy volunteers of the anesthetic propofol on brain uptake of this PET radioligand targeting translocator protein and discuss implications for cognitively impaired patients requiring anesthesia for PET imaging. . . . . ***Page 64***

PiB and florbetapir: Landau and colleagues compare ^{11}C-Pittsburgh compound B and ^{18}F-florbetapir amyloid-β PET imaging in cognitively normal older adults and patients with mild cognitive impairment and Alzheimer disease and describe methods for standardizing and correlating results with the 2 tracers. . . . . ***Page 70***

Imaging synaptic acetylcholine: Esterlis and colleagues examine whether β_2-nicotinic acetylcholine receptor binding of ^{123}I-5-IA on SPECT is sensitive to increases in extracellular levels of acetylcholine in humans. . . . . ***Page 78***

Quantitative SPECT: Bailey and Willowson provide an educational overview of evidence-based reports on quantitative SPECT imaging and potential clinical applications. . . . . ***Page 83***

PET and primary brain tumors: Evans and colleagues apply an ^{89}Zr-labeled derivative of transferrin in animal PET studies designed to provide a more detailed identification of multiple types of tumor tissue in the brain. . . . . ***Page 90***

Multimodal imaging nanophosphor: Lee and colleagues describe synthesis and initial evaluation of a ^{124}I-labeled nanoparticle with promise for combined PET/MR/optical imaging in tumor angiogenesis and cancer-specific diagnoses. . . . . ***Page 96***

^{99m}Tc-peptide and treatment response: Song and colleagues determine the effectiveness of SAAC(^{99m}Tc)-PSBP-6, a small-molecular-weight peptide, in PET detection of apoptosis induced by chemotherapy and review the tracer's potential as a substitute for ^{18}F-FDG. . . . . ***Page 104***

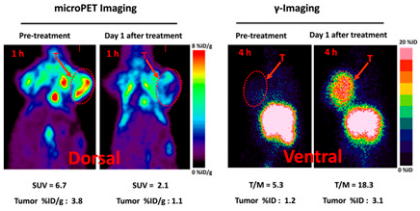

^{166}Ho-MSNs for radionuclide therapy: Di Pasqua and colleagues explore the utility of mesoporous silica nanoparticles as a carrier material for the stable isotope ^{165}Ho and its subsequent radionuclide, ^{166}Ho, in therapy for ovarian cancer metastasis. . . . . ***Page 111***

^{18}F-FSPG PET in HCC: Baek and colleagues investigate the tumor detection rate of this PET tracer, which assesses specific cysteine/glutamate exchange transporter activity, in patients with hepatocellular carcinoma. . . . . ***Page 117***

Folic acid–targeted radionuclide therapy: Müller and colleagues detail a strategy in which a DOTA–folate conjugate with an albumin-binding entity was developed to prolong circulation in the blood and potentially improve tumor-to-kidney ratios for radiotherapy. . . . . ***Page 124***

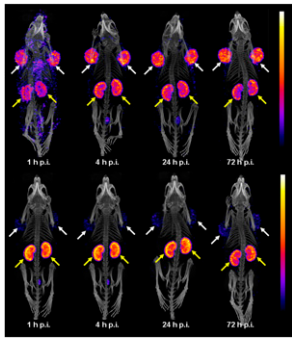

Improving PET kinetic modeling: Alf and colleagues test the feasibility of input function measurement with an arteriovenous shunt and a coincidence counter in mice and compare the method with an image-derived input function. . . . . ***Page 132***

Imaging imidazoline-I_2 binding sites: Kealey and colleagues use ^{11}C to radiolabel a promising ligand compound for PET imaging of I_2 brain binding sites in vivo in mice. . . . . ***Page 139***

PET in cell therapy after stroke: Miyamoto and colleagues determine whether ^{18}F-FDG PET can serially monitor the beneficial effects of transplanted bone marrow stromal cells on cerebral glucose metabolism in rat brain after induced ischemic stroke. . . . . ***Page 145***

^{18}F-FLT PET and experimental RA: Fuchs and colleagues study the feasibility of measuring cell proliferation noninvasively in vivo in mice during different stages of experimental arthritis using ^{18}F-FLT PET. . . . . ***Page 151***

Elucidating renal ^{99m}Tc-DMSA uptake: Weyer and colleagues use megalin/cubilin–deficient mice produced by gene knockout to determine whether receptor-mediated endocytosis is responsible for renal uptake of ^{99m}Tc-DMSA. . . . . ***Page 159***

ON THE COVER

Representative views of MR imaging, PET, and digital autoradiography highlight the exceptional avidity of ^{89}Zr-transferrin for an orthotopic glioblastoma multiforme tumor.

See page 90.